Electron diffraction, X-ray powder diffraction and pair-distribution-function analyses to determine the crystal structures of Pigment Yellow 213, C₂₃H₂₁N₅O₉

Martin U. Schmidt,[a]* Stefan Brühne,[a,b] Alexandra K. Wolf,[a] Anette Rech,[a] Jürgen Brüning,[a] Edith Alig,[a] Lothar Fink,[a] Christian Buchsbaum,[a] Jürgen Glinnemann,[a] Jacco van de Streek,[a] Fabia Gozzo,[c] Michela Brunelli,[d] Frank Stowasser,[e] Tatiana Gorelik,[f] Enrico Mugnaioli[f] and Ute Kolb[f]

[a]Goethe Universität, Institut für Anorganische und Analytische Chemie, Max-von-Laue-Strasse 7, 60438 Frankfurt am Main, Germany, [b]Goethe Universität, Physikalisches Institut, Max-von-Laue-Strasse 1, 60438 Frankfurt am Main, Germany, [c]Swiss Light Source, Paul Scherrer Institut, PSI 5232 Villigen, Switzerland, [d]Euro-European Synchrotron Radiation Facility, BP 220, 38043 Grenoble CEDEX, France, [e]Novartis Pharma AG, Inhalation Development and Technology, 4002 Basel, Switzerland, and [f]Institut für Physikalische Chemie, Johannes Gutenberg Universität Mainz, Welderweg 11, 55099 Mainz, Germany

Correspondence e-mail: m.schmidt@chemie.uni-frankfurt.de

The crystal structure of the nanocrystalline α phase of Pigment Yellow 213 (P.Y. 213) was solved by a combination of single-crystal electron diffraction and X-ray powder diffraction, despite the poor crystallinity of the material. The molecules form an efficient dense packing, which explains the observed insolubility and weather fastness of the pigment. The pair-distribution function (PDF) of the α phase is consistent with the determined crystal structure. The β phase of P.Y. 213 shows even lower crystal quality, so extracting any structural information directly from the diffraction data is not possible. PDF analysis indicates the β phase to have a columnar structure with a similar local structure as the α phase and a domain size in column direction of approximately 4 nm.

1. Introduction

Some years ago, the automotive industry switched from solvent-based to water-based coatings. This led to the need for new, water-dispersible pigments. Greenish-yellow shades appeared to be one of the most problematic, because all existing greenish-yellow pigments were either not dispersible in water (*i.e.* they showed severe agglomeration and aggregation) or had an insufficient weather fastness, *i.e.* they faded out after a few years. Moreover, clear greenish-yellow shades cannot be achieved by mixing green and yellow pigments, since this would lead to dull shades.

Under these demands one company (Clariant GmbH) developed Pigment Yellow 213 (P.Y. 213, Fig. 1) as a new compound for water-based coatings (Stengel-Rutkowski & Metz, 2001). P.Y. 213 exists in (at least) two polymorphs: the brown β phase is formed as an intermediate product during synthesis. Subsequent heating in organic solvents to 423–473 K results in the greenish-yellow (lemon-yellow) α phase (Fig. 2). The α phase shows good weather fastness and it does not agglomerate in water. Currently the α phase is industrially used for water-based car coatings.
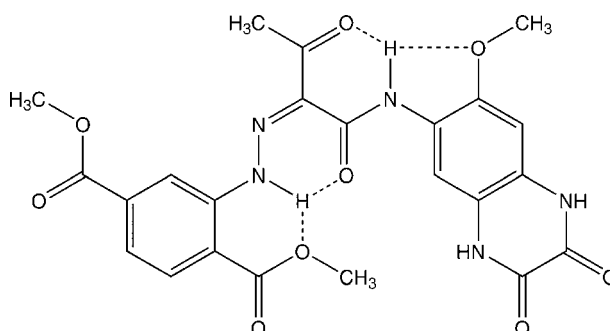

Figure 1
Pigment Yellow 213 (P.Y. 213, C₂₃H₂₁N₅O₉).

During the development of P.Y. 213, dozens of similar compounds with other substitution patterns were tested; all had either a dull shade or a worse light stability. It was observed that the colour and properties of these pigments depend not only on the molecular constitution, but also, and strongly, on the solid-state structure – as can be seen *e.g.* by the colour differences between the yellow α phase and the brown β phase of P.Y. 213. It is obvious that the crystal structure of the α phase of P.Y. 213 is responsible for its outstanding properties.

Although P.Y. 213 is industrially produced, its crystal structures are not known. All attempts to grow single crystals failed, since the pigment is hardly soluble at all in water or organic solvents, even at temperatures of 473 K. Crystal growth from the melt or by sublimation is not possible either, because the pigment melts at 642 K with decomposition and does not sublime. The crystallinity of the α phase of P.Y. 213 is never really good, and thus the X-ray powder data are always of so limited quality that the peaks cannot be reliably indexed.

After considerable effort in synthesis, recrystallization, X-ray powder diffraction, electron diffraction and lattice-energy minimization, we were able to determine the crystal structure of the α phase of P.Y. 213 by combining electron diffraction and X-ray powder diffraction methods.

The powder diagram of the β phase of P.Y. 213 shows no well defined Bragg reflections at all. Nevertheless, the humps in the X-ray powder diagram still contain some information, which can be analysed by total scattering methods, especially the analysis of the atomic pair-distribution function (PDF).

PDF analyses have long been used for liquids, glasses, fibres and other disordered, amorphous or nanocrystalline inorganic compounds (Billinge & Kanatziolis, 2004) as well as for quasicrystals (Brühne *et al.*, 2006). However, molecular compounds have rarely been investigated by PDF analyses; examples include C_{60} (Juhas *et al.*, 2006) and a few pharmaceutical compounds (Bates & Ivanisevic, 2005; Nollenberger *et*

Figure 2
Pigment Yellow 213: powders of the α phase (greenish-yellow) and the β phase (brown).

al., 2009). Here, to our knowledge, the PDF technique is applied to an organic pigment for the first time.

2. Experimental

2.1. Synthesis and crystallization experiments

P.Y. 213 was synthesized by azo coupling in water (Herbst & Hunger, 2004).

The crystallinity of the α phase could be improved by heating a suspension in *N*-methylpyrrolidone to 423 K for 3 h with subsequent recrystallization from large amounts of boiling DMSO at 462 K; alternatively the pigment could be treated with a melt of benzoic acid (m.p. 395 K). Different analytical methods (DSC, DTA/TG, IR, elemental analysis) proved that the α phase consists of P.Y. 213 molecules only, without any water or solvent molecules in the crystal lattice.

2.2. X-ray powder diffraction

2.2.1. In-house. Powder diffraction of both the α and β phases of P.Y. 213 were performed with Cu $K\alpha_1$ radiation (λ = 1.5406 Å) using a STOE Stadi-P diffractometer in transmission mode. The samples were placed in glass capillaries 0.7 mm in diameter and spun, or prepared between two Mylar® films and rotated during the measurements. Measurements were also carried out at lower temperatures (80–250 K).

2.2.2. Synchrotron. Synchrotron X-ray powder diffraction experiments (SR-XRPD) were performed at the Swiss Light Source Materials Science beamline (SLS-MS) at Paul Scherrer Institut and at the ID 31 beamline at the European Synchrotron Radiation Facility (ESRF).

At the SLS-MS powder station, with a high resolution and a high counting rate, diffraction patterns for Rietveld refinement were collected on the α phase at λ = 0.92571 (3) Å, as a function of temperature (from 100 to 300 K with 50 K steps) using the silicon microstrip detector MYTHEN I (Gozzo *et al.*, 2004; Schmitt *et al.*, 2004).

At the ESRF-ID31 high-resolution PD beamline, experiments for the analysis of the PDF on the α and β phases were performed at 30.73 keV photon energy [λ = 0.40007 (7) Å] and the powder pattern was collected up to $2\theta = 120°$ using the multicrystal analyser detector. To ensure good counting statistics at high 2θ values, a variable counting-time scheme (VCT) was adopted (Shankland *et al.*, 2004). The total acquisition time for each phase was 8 h.

All experiments were performed in Debye–Scherrer (transmission) geometry using cylindrical borosilicate 0.5 mm diameter capillaries which were spun for improved powder averaging.

2.3. Indexing attempts and LeBail fits

For extracting the peak positions and indexing the powder patterns of the α phase, various programs were used, including the STOE *WinX^POW* suite (STOE & Cie, 2004) with *ITO* (Visser, 1969), *TREOR* (Werner *et al.*, 1985) and *DICVOL* (Boultif & Louër, 1991), *McMaille* (LeBail, 2004), the *Crysfire/Checkcell* suite (Shirley, 2006), the *DASH* suite (David *et al.*,

2006) and *TOPAS* (Coelho, 2006). All resulting unit cells were transformed to the standard setting (for triclinic: $a \leq b \leq c$; α, β, γ all > 90° or all < 90°).

Subsequent LeBail fits were carried out with *GSAS* (Larson & von Dreele, 1994).

2.4. Electron diffraction

Samples of the α and β phases were prepared for transmission electron microscopy (TEM) by suspending the pigment powders in ethanol in an ultrasonic bath. A drop of the suspension was placed on a carbon film with underlying copper grid and dried in air. TEM investigations were performed on a TECNAI F30 ST transmission electron microscope with a field-emission gun, scanning unit (STEM), high angular annular dark-field detector (HAADF) and a 10 µm C2 aperture for nano electron diffraction (NED). STEM images were obtained in µ-probe mode, accepting a lower resolution to allow the sequential recording of NED patterns. Electron-diffraction data were collected using a double-tilt rotational holder (GATAN) as well as a tomography holder (FISCHIONE) within a tilt range of ± 30° in two ways, firstly by manual tilt of a crystal around a low-index crystallographic axis (Kolb & Mateeva, 2003) and secondly by a recently developed automated diffraction tomography (ADT) module (Kolb *et al.*, 2007, 2008).

2.5. Prediction of possible crystal structures by lattice-energy minimizations

For α-P.Y. 213, calculations were performed with *CRYSCA* (Schmidt & Kalkhof, 1997) in $P\bar{1}$ with lattice parameters obtained by electron diffraction; additional calculations were performed with variable lattice parameters in various space groups.

2.6. Structure solution of the α-phase from X-ray powder data by real-space methods

At first a Pawley fit was performed (*TOPAS*). The resulting, more accurate lattice parameters were used for structure solution with *TOPAS*. The Pawley refinement had indicated the presence of anisotropic peak broadening.
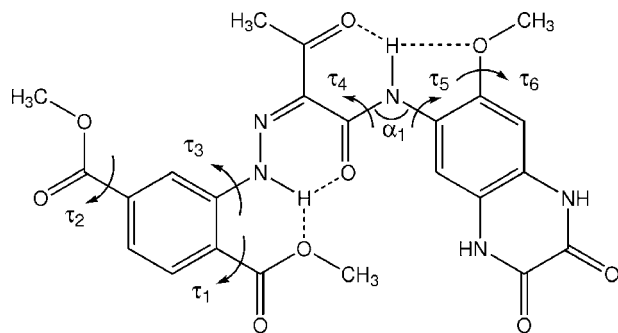

Figure 3
Intramolecular degrees of freedom: The torsion angles τ_1–τ_3 and τ_5–τ_6 were treated as variable during the structure solution by real-space methods. In the lattice-energy minimizations additionally τ_4 and α_1 were varied.

The molecular structure was calculated using the Dreiding force field (Mayo *et al.*, 1990). The molecular geometry was set up as a rigid body with the exception that five torsion angles of the molecule were refined independently during the calculations (Fig. 3). The torsion angles were not constrained to any ranges. First calculations were undertaken using the space group $P\bar{1}$ ($Z = 2$).

All calculations were performed in real space by a combination of Monte-Carlo and simulated-annealing methods. The X-ray powder diffraction patterns were directly used without prior intensity extraction. Refined parameters during the minimization were the rotational and positional parameters of the rigid body, selected torsion angles and the scaling factor (altogether 12 parameters). Lattice parameters, profile and background parameters were kept fixed at values from the Pawley refinement in order to speed up the calculations. The global optimization procedure was repeated until the minimization routine showed several low minima at comparable levels after 2000 cycles taking all-in-all 4 h calculation time on a 3 GHz computer. It has to be pointed out that the anisotropic peak broadening and preferred orientation were not taken into account during these calculations; however, a fit that is very good visually to the data had been achieved. The resulting best model was considered further.

2.7. Rietveld refinement of the α phase

The Rietveld refinement of the α phase was performed with the program *TOPAS*. For the room-temperature structure, synchrotron data with a wavelength of $\lambda = 0.40$ Å were chosen, because they showed only a small degree of preferred orientation. Data out to $2\theta = 18.75°$ were used, which corresponds to a real-space resolution of 1.23 Å. For the temperature-dependent refinements, synchrotron data with $\lambda = 0.92571$ Å were used.

Suitable chemical restraints were added for all bond lengths, valence angles and the planarity of all aromatic systems. In the last step of the Rietveld refinement, all parameters were allowed to refine simultaneously.

The laboratory data had shown that the preferred orientation mainly affects the strong (211) reflection (at ∼ 27° for Cu $K\alpha$). Therefore, also for the synchrotron data a respective preferred orientation correction using the March–Dollase expression (March, 1932; Dollase, 1986) was included.

2.8. Generation of PDFs

The measured $2\theta_{max}$ of 120° at $\lambda = 0.40$ Å corresponds to a maximal scattering-vector length of ∼ 30 Å^{-1}. The background was determined from the measurement of an empty capillary and subtracted. Data corrections, normalization and generation of PDFs were performed using the software *PDFgetX*2 (Qiu *et al.*, 2004).

Since the sample consisted exclusively of weak scatterers, only data up to $Q_{max} = 15$ Å^{-1} could be used to generate clean $G(r)$ functions.

3. Results and discussion

3.1. α phase

3.1.1. Synthesis and crystallization experiments. The crystallinity of α-P.Y. 213 could be improved by recrystallizing P.Y. 213 from boiling DMSO and suspension treatment in molten benzoic acid. The resulting powder diagram is shown in Fig. 4.

3.1.2. Indexing attempts and LeBail fits. Indexing was extensively tried on different laboratory and synchrotron X-ray powder diagrams from different samples. Various triclinic and monoclinic unit cells were suggested, but it was not possible to determine which was the correct one. Even extensive LeBail fits with *GSAS* did not help: LeBail fits with considerably different uni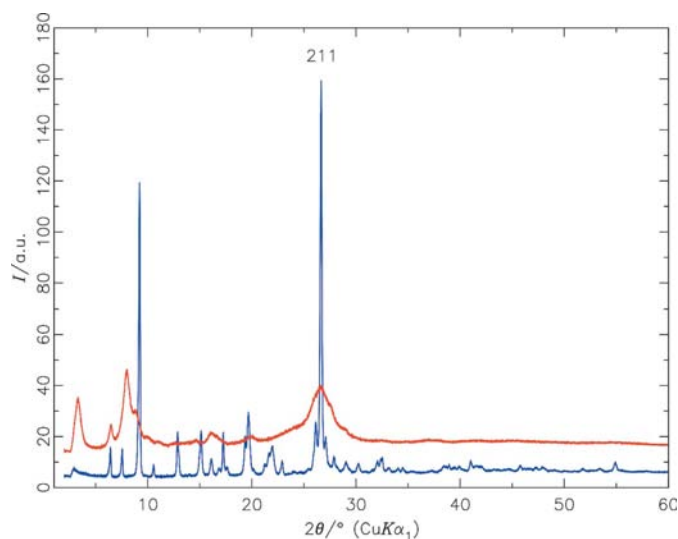t cells gave similar R values, but none of the fits were really convincing. Therefore, we used electron diffraction to determine the lattice parameters.

3.1.3. Determination of lattice parameters by electron diffraction. The crystallites of α-P.Y. 213 are platelets with a lateral size of 0.5–2 μm (Fig. 5). The material was fairly stable under electron radiation: the crystals could tolerate an electron dose rate of 10–15 e $\mathring{A}^{-2}$ s^{-1}.

Electron-diffraction patterns were collected around several low-index axes by manual tilt. Fig. 6 shows two selected patterns of the main crystallographic zones [001] and [010], from which the reciprocal lattice parameters a^*, b^*, c^*, β^* and γ^* could be measured directly. Using least-squares refinement (*CRISP;* Hovmöller, 1992) to minimize the statistical error in the angle determination, the values for β^* and γ^* could be determined with an error of less than 0.5°. Due to the platelet morphology, the crystallites have a strong preferred orientation, therefore the [100] crystallographic zone was not accessible, and the angle α^* could not be measured directly. Its value was determined from Vainstein plots (Vainstein, 1964; Kolb & Gorelik, 2005) built from three-dimensional diffraction data. The corresponding lattice parameters in direct space are listed in Table 1.

Alternatively, the lattice parameters were accessed through a tilt (tilting interval of ± 30°, step size of 1°) of the crystal around an arbitrary axis, whereby diffraction patterns were collected automatically using an automated diffraction tomography (ADT) module. Fig. 6(*c*) shows an integrated diffraction volume viewed along the [001] direction: periodic rows of reflections are clearly seen. After the data were carefully examined for consistency, unit-cell parameters were determined using the previously reported procedure (Kolb *et al.*, 2008). The parameters found from ADT data are included in Table 1. The determined parameters are comparable with those obtained by manual tilting. Apparently, the α angle is still difficult to determine precisely.

3.1.4. Prediction of possible crystal structures by lattice-energy minimizations. In our attempts to solve the crystal structure of α-P.Y. 213, we predicted structures using global lattice-energy minimization. This procedure has repeatedly been used to solve organic crystal structures from unindexed X-ray powder data (Hofmann & Kuleshova, 2005; Schmidt *et al.*, 2005, 2006*a*,*b*; Paulus *et al.*, 2007).

For P.Y. 213, one of the resulting low-energy structures looked promising in terms of molecular packing and intermolecular hydrogen bonds, and had a simulated powder diagram similar to the experimental diagram of the α phase. The subsequent Rietveld refinement with *GSAS* converged with a nearly acceptable fit. However, a

Figure 4
Pigment Yellow 213: X-ray powder diagrams of the α phase (blue, lower line) and the β phase (red, upper line); Cu $K\alpha_1$ radiation, λ = 1.5406 Å. This figure is in colour in the electronic version of this paper.
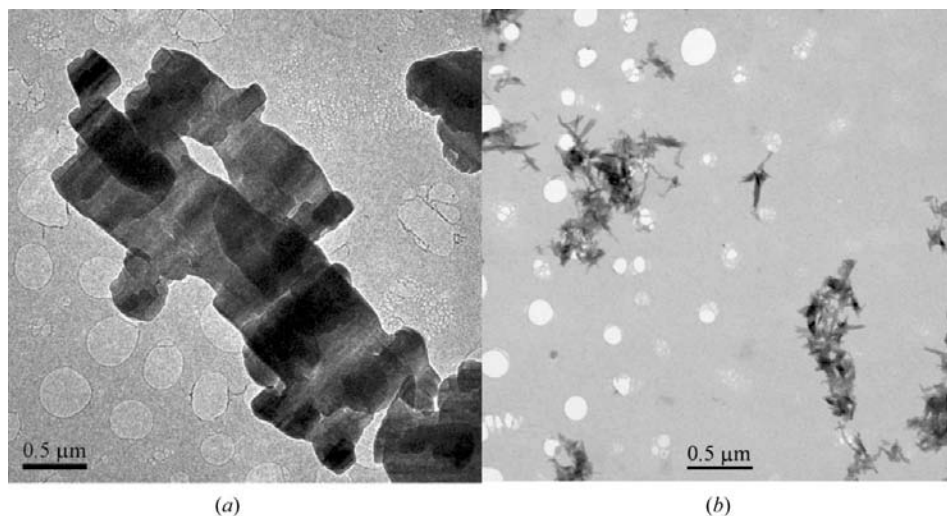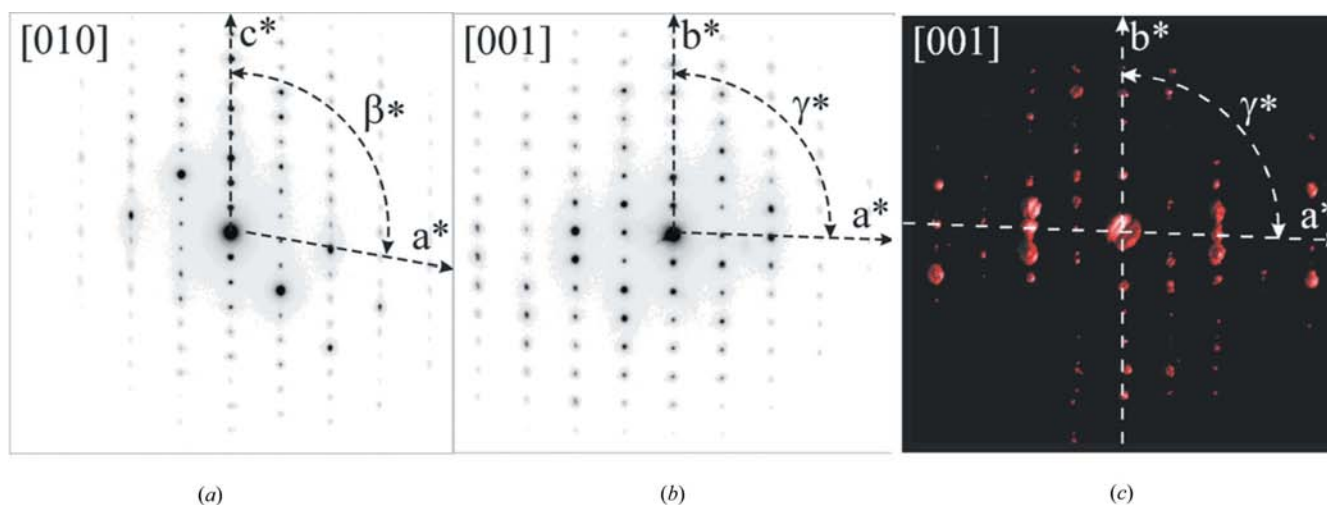

Figure 5
(*a*) TEM photograph of α-P.Y. 213. The platelet morphology is apparent; (*b*) μ-STEM image (inverted) of β-P.Y. 213 with needle-shaped crystals.

Figure 6
Electron-diffraction patterns of α-P.Y. 213: (a) [010] zone; (b) [001] zone; (c) three-dimensional fully integrated automated diffraction tomography (ADT) data projected along the c^* direction.

Table 1
Lattice parameters of α-P.Y. 213 at 293 K.

	Electron diffraction, manual tilting	Electron diffraction, automated diffraction tomography (ADT)	Final values from Rietveld refinement
a (Å)	6.83	7.0 (3)	6.9006 (3)
b (Å)	11.86	11.6 (6)	11.8347 (6)
c (Å)	14.31	13.8 (2)	14.0592 (7)
α (°)	ca 77	81.5	81.811 (4)
β (°)	79.7	78.7	81.032 (9)
γ (°)	86.1	86.3	87.542 (1)
V (Å^3)	1114	1045	1122.32 (1)
Space group	$P1$ or $P\bar{1}$	$P1$ or $P\bar{1}$	$P\bar{1}$
Z	2	2	2

Errors in lattice parameters from ADT were calculated by the standard deviation of the cluster centre and refined vector position.

Rietveld refinement is not always definite proof for the correctness of a crystal structure, especially if the powder data are of limited quality (Buchsbaum & Schmidt, 2007). For α-P.Y. 213 a comparison of simulated and experimental electron-diffraction intensities revealed that the calculated structure was not the correct one.

After the structure had been solved by *TOPAS* (see §3.1.5), it turned out that the lattice-energy minimizations failed because the molecule shows an unusual conformation which was not included in the minimizations. This results in a different molecular shape, which considerably changes the crystal structure and the lattice energies.

3.1.5. Structure solution from X-ray powder data by real-space methods. The crystal structure of the α phase could finally be solved by real-space methods using recent developments of the program *TOPAS*. The quality of the laboratory data turned out to be fully sufficient. From the various indexing suggestions, one was chosen which had lattice parameters similar to the values obtained by electron-diffraction data (it was the indexing from *DASH/DICVOL* and *TOPAS*

on laboratory data). Although the LeBail fit with *GSAS* was not convincing, the Pawley fit with *TOPAS* converged with good agreement factors ($\chi^2 = 0.020$, $R'_{wp} = 0.072$, $R'_p = 0.073$; the prime indicates background-subtracted values). The structure solution trials converged with $\chi^2 = 5.4$, $R'_{wp} = 0.227$, $R'_p = 0.219$ (background-subtracted values). The resulting molecular conformation was not the expected one: the COOCH$_3$ group neighbouring the NH group rotated by 180°. In order to test the obtained structure, individual torsion angles of the molecule were rotated by 180° off their orientation and the minimization was repeated; for τ_1 (COOCH$_3$ group) refinements were even carried out in steps of 30°. In no case was a lower minimum obtained, thus proving the overall conformation to be the correct one.

3.1.6. Rietveld refinement. For the Rietveld refinement, synchrotron data were used. The refinement converged with a smooth difference curve with $\chi^2 = 1.34$, $R_{wp} = 0.0312$ and $R_p = 0.0238$ (without background subtraction), $R'_{wp} = 0.1746$ and $R'_p = 0.2610$ (after background subtraction). The Rietveld plot is shown in Fig. 7. Crystallographic data are given in Table 2. Atomic coordinates are given in the supplementary material.[1]

Ultra-high-resolution powder diffraction patterns measured at ESRF-ID31 with $\lambda = 1.53494$ (4) Å showed strong aniso-tropic peak broadening; this points to anisotropic domain sizes, as it is frequently observed in organic pigments and other solids with large, almost planar molecules.

The temperature-dependent high-resolution synchrotron data of the α phase collected at SLS showed no phase transition between 100 and 300 K, which confirms the results obtained from the in-house data. Rietveld refinements were made on all datasets (Table 3). The molecular arrangement changed very slightly with decreasing temperature; however, the overall packing arrangement remained the same and the

Table 2
Experimental data for α-P.Y. 213 (Rietveld refinement at 293 K).

Crystal data	
Chemical formula	$C_{23}H_{21}N_5O_9$
M_r	511.45
Crystal system, space group	Triclinic, $P\bar{1}$
Temperature (K)	293
a, b, c (Å)	6.9006 (3), 11.8347 (6), 14.0592 (7)
α, β, γ (°)	81.811 (4), 81.032 (9), 87.541 (10)
V (Å³)	1122.31 (10)
Z	2
Radiation type	Synchrotron
Wavelength of incident radiation (Å)	0.40007
μ (mm⁻¹)	0.03
Specimen shape, size (mm)	Cylinder, 10 × 0.5
Data collection	
Diffractometer	High resolution (ID31, ESRF)
Specimen mounting	Borosilicate capillary
Scan method	Continuous
Data-collection mode	Transmission
2θ values (°)	$2\theta_{min} = 1.300$, $2\theta_{max} = 18.750$, $2\theta_{step} = 0.005$
Refinement	
$R_p, R_{wp}, R_{exp}, \chi^2$	0.261, 0.175, 0.130, 1.80
Excluded region(s)	None
No. of data points	5356
No. of parameters	1375
No. of restraints	159

Table 3
Temperature dependence of the lattice parameters of α-P.Y. 213 determined by Rietveld refinement.

	100 K	200 K	300 K
a (Å)	6.7716 (1)	6.8326 (1)	6.9034 (2)
b (Å)	11.7653 (3)	11.7988 (3)	11.8358 (3)
c (Å)	14.0269 (4)	14.0483 (3)	14.0628 (3)
α (°)	82.209 (2)	81.997 (2)	81.796 (2)
β (°)	81.394 (4)	81.155 (4)	81.016 (3)
γ (°)	88.394 (4)	87.968 (5)	87.526 (5)
V (Å³)	1094.72 (5)	1108.04 (4)	1123.06 (5)

neighbouring molecule, resulting in an eight-membered ring across an inversion centre, as is frequently found for *cis*-amide systems, *e.g.* in benzimidazolones (van de Streek *et al.*, 2009). The other NH group of the quinoxalinedione moiety forms a second intermolecular hydrogen bond to a C=O of the acetyl fragment (Fig. 8). The remaining two NH groups form intramolecular hydrogen bonds to carbonyl groups, as is always found for yellow azo pigments with acetoacetyl groups. The intermolecular hydrogen bonds connect the molecules into double chains running in the [01$\bar{1}$] direction. The chains arrange in layers parallel to the (211) plane, with a layer distance of 3.34 Å (Fig. 9). It is this layer arrangement which causes the strong intensity for the (211) peak in the X-ray powder diagram. Molecules of successive layers are stacked on top of each other, but rotated by 180°, and form columns along the [100] direction. The layers are connected by van der Waals and Coulomb interactions.

The most remarkable feature of the crystal structure is the rare molecular conformation with an NH group forming an intramolecular hydrogen bond to the OCH₃ fragment of the COOCH₃ group (as shown in Fig. 1). In the Cambridge Structural Database (CSD; Allen, 2002) there are 32 struc-
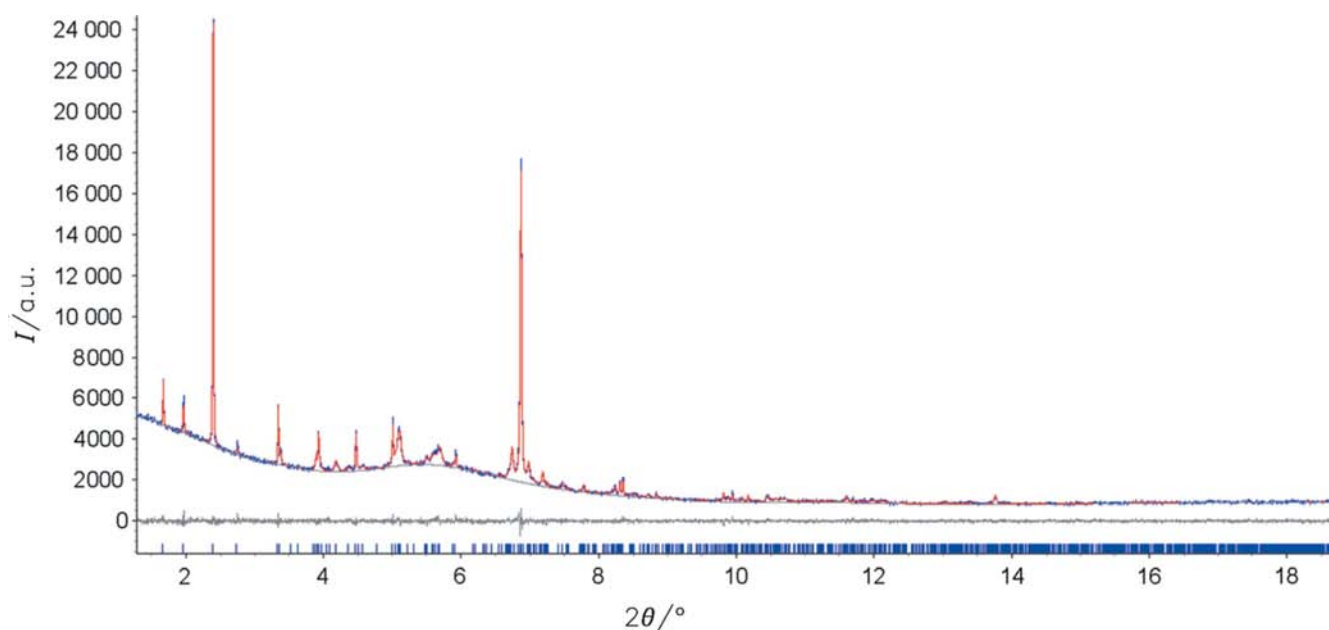
variations observed are just due to the volume contraction of ∼ 2.5% between 300 and 100 K.

3.1.7. Crystal structure of the α phase. The α polymorph of P.Y. 213 crystallizes in $P\bar{1}$, $Z = 2$. The molecule is almost planar. There are two intermolecular hydrogen bonds, both involving the NH groups of the two *cis*-amide fragments of the quinoxalinedione fragment: one of the NH groups forms an intermolecular hydrogen bond with a C=O group of a

Figure 7
Rietveld plot of α-P.Y. 213 (λ = 0.40 Å). Calculated (red), observed (blue), and difference (black, below) profiles are shown. Reflection positions are shown as blue tick marks. This figure is in colour in the electronic version of this paper.

tures with NH groups neighbouring a COOCH$_3$ group; in all cases, a hydrogen bond to the C=O fragment is formed. Fig. 8 suggests that this unusual conformation of P.Y. 213 is necessary to allow close packing: If the COOCH$_3$ group were rotated by 180°, there would be an awkward gap in the crystal structure that would be difficult to fill.

Fig. 8 also gives an explanation for the role of the COOCH$_3$ and OCH$_3$ groups in the crystal structure: These substituents allow for an efficient packing: Changing *e.g.* the position of the COOCH$_3$ or OCH$_3$ groups or substituting *e.g.* one of the COOCH$_3$ groups by a COOC$_2$H$_5$ group would result in steric hindrance and consequently in a less dense packing. It is this efficient, dense packing which explains the observed good fastness properties of P.Y. 213.

3.2. β phase

The β phase of P.Y. 213 is a brown, metastable, nanocrystalline powder (see Fig. 5b). The powder diagram is included in Fig. 4. All recrystallization attempts failed: either the crystallinity did not change or the powder transformed to the more stable α phase. Due to the low crystallinity of the β phase, no indexing of the powder-diffraction data was attempted.

No reliable information has yet been obtained by electron diffraction.

Crystal-structure predictions were made by lattice-energy minimizations with variable lattice parameters in various space groups, but it was not possible to select which of the calculated structures actually corresponds to the β phase.
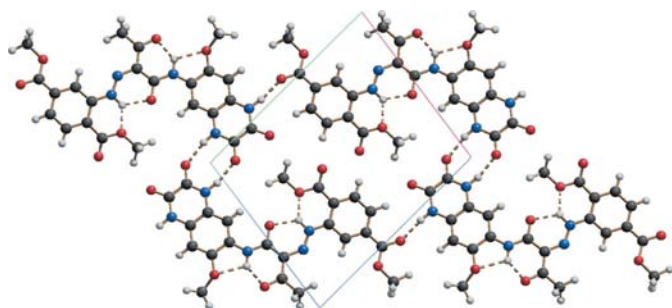

Figure 8
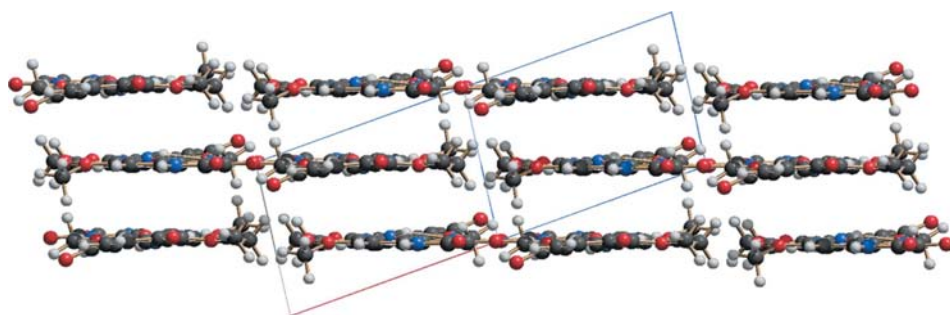Crystal structure of the α phase of P.Y. 213. View along [100].

Figure 9
Crystal structure of the α phase of P.Y. 213. View along [01$\bar{1}$], showing the layer arrangement.

To obtain structural information on the β phase, we used the pair-distribution-function analysis.

3.3. Pair-distribution-function analysis of the α and β phases

3.3.1. PDF analysis of the α phase. The atomic pair-distribution function (PDF) represents the probability to find two atoms separated by a distance r (Egami & Billinge, 2003).

For the PDF analyses of α-P.Y. 213, high-resolution synchrotron data were used (Figs. 10a and b). After data correction and normalization, the reduced structure function $F(Q)$ was obtained, see Fig. 10(c). This figure reveals similarities in $F(Q)$ for the α and β polymorphs of P.Y. 213 which are not revealed by conventional (not normalized, low Q) powder diffractograms $I(Q)$: the general appearances of the two curves with Q and the oscillations are clearly related.

The PDF of the α phase of P.Y. 213 is shown in Fig. 11(a). The first peak includes the C—C, C—O and C—N distances, the second peak the 1,3- and 1,4-distances. From the third peak on, intermolecular distances are also included. The characteristic feature is an oscillation of the PDF with a period of ∼ 3.3 Å. This feature is caused by the molecular stacking: The distance between neighbouring molecules in a column is ∼ 3.3 Å; this distance occurs for many atoms and consequently dominates the PDF. Perpendicular to the column direction, the distribution of atom–atom distances is more homogeneous and does not lead to a pronounced feature in the PDF.

The oscillation in the PDF still persists at $r = 100$ Å (Fig. 11a). This indicates a long-range translational order in the column direction, which is also confirmed by the small peak width of the (211) reflection.

For quantitative analysis, model PDFs can be simulated using (1)

$$G(r)_{\text{calc}} = \frac{1}{r}\sum_i\sum_j\left[\frac{f_if_j}{\langle f\rangle^2}\times\delta(r-r_{ij})\right]-4\pi r\rho_0, \quad (1)$$

where f_i is the scattering factor of atom i and $\langle f\rangle^2$ is the average scattering power of all atoms in the sample.

For a PDF refinement a reliability factor is defined by

$$R_{\text{PDF}} = \left\{\frac{\sum_{i=1}^N[G_{\text{obs}}(r_i)-G_{\text{calc}}(r_i)]^2}{\sum_{i=1}^N G_{\text{obs}}^2(r_i)}\right\}^{1/2}. \quad (2)$$

R values of PDF refinements should never be mistaken for R values from Rietveld or single-crystal structure refinements!

The least-squares refinement software *PDFFIT* (Proffen & Billinge, 1999) was employed to fit the model PDF of the α phase to the experimental one using the crystal structure determined from X-ray powder data as a structural model. At present a PDF fit for organic molecules is hampered by

Table 4
PDF refinement parameters for α- and β-P.Y. 213 obtained with *PDFFIT*, different r ranges, datasets at Q_{max} = 15 Å^{-1}; r_{cut} = 1.8 Å; δ and φ describe the PDF peak width.

Phase	r range (Å)	R	Scale factor	δ	φ
α	0.8–32.0	0.389	0.83 (3)	0.29128 (4)	0.840 (13)
	0.8–4.0	0.406	0.97 (4)	0.29131 (2)	0.832 (7)
	0.8–7.0	0.452	0.99 (4)	0.29125 (3)	0.852 (10)
	0.8–10.0	0.469	0.88 (4)	0.29141 (3)	0.800 (7)
	0.8–13.0	0.465	0.88 (4)	0.29141 (3)	0.834 (9)
	13.0–32.0	0.234	0.8 (3)	1 (6)	0.8
β	0.8–4.0	0.391	1.05 (5)	0.29131 (2)	0.832 (7)
	0.8–7.0	0.463	0.98 (5)	0.29121 (4)	0.863 (13)
	0.8–10.0	0.485	0.92 (5)	0.29125 (4)	0.850 (13)
	0.8–13.0	0.561	0.84 (5)	0.29133 (4)	0.823 (13)

the fact that (to our knowledge) all PDF software is dedicated to inorganic materials and cannot yet handle rigid bodies, constraints or restraints, which are required for the refinement of organic compounds. Therefore, we refined only a scale factor, and two parameters describing the PDF peak width (Jeong *et al.*, 1999). All lattice, positional and displacement parameters were fixed to the values obtained from the Rietveld refinement.

The model PDF could be fitted to the measured $G(r)_{exp}$ for 0.8 Å $< r <$ 32 Å with an accuracy of R_{PDF} = 0.389. The resulting fit is shown in Fig. 11(b). The refinements are summarized in Table 4.

Closer inspection of the fit in Fig. 11(b) reveals that there is a larger difference for $r <$ 13 Å. Consequently, the r range was split into two ranges, 0.8 $< r <$ 13 and 13 $< r <$ 32 Å. Now R_{PDF} values are 0.465 for the low-r region and 0.234 for the high r region (Fig. 11c). We conclude here that the *average* long-range packing of the molecules is as found by Rietveld analysis. The long-range averaging is accounted for by a δ value increased about by a factor of three. Assignment of different displacement parameters to groups of atoms did not improve the fit. It would be very advantageous to make a combined Rietveld and PDF fit including restraints for the molecular structure, but the software has still to be developed.

3.3.2. On the structure of the β phase. The β phase shows only a few broad peaks in the X-ray powder pattern (Fig. 4), nevertheless, the PDF contains valuable real-space information on the *local* atomic structure. Fig. 12(a) plots the PDF up to r = 100 Å. Two features are apparent:

(i) The PDF oscillates with a period of $\sim$ 3.3 Å, as for the α phase.

(ii) In contrast to the α phase, the PDF of the β phase is damped to zero beyond $r \simeq$ 40 Å.

Consequently, the molecules in the β phase should form columnar stacks as in the α phase, but with a reduced coherence length: after 30–40 Å – *i.e.* about 10 molecules – the translational order in column direction is interrupted either by a crystal surface or by a severe lattice defect. Correspondingly, the X-ray powder diagram does not show a sharp peak at $d \simeq$ 3.3 Å (corresponding to $2\theta = 7°$ for λ = 0.4 Å), but a broad hump whereas the α phase shows a sharp peak. For large, almost planar molecules like P.Y. 213 the domain sizes are

frequently strongly anisotropic, which is reflected in the occurrence of both broader and sharper peaks in the powder
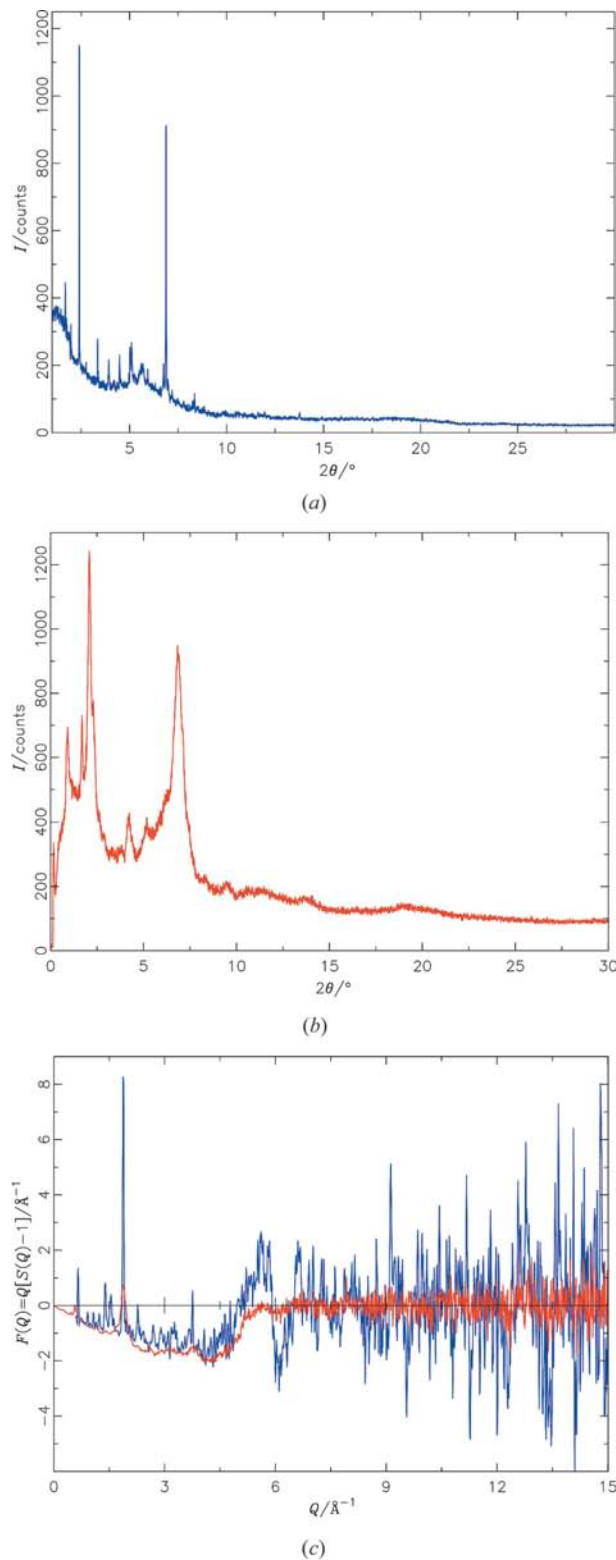

Figure 10
Synchrotron X-ray powder diffraction data used for the PDF analyses, measured with λ = 0.40007 (7) Å. (a) α phase; (b) β phase; (c) normalized structure function $F(Q)$ for the α phase (blue) and the β phase (red); note that the abscissa is Q in Å^{-1}. The similar general behaviour of the curves $F(Q)$ with Q for α and β phases is apparent.

pattern. At lower 2θ angles (1–2° for $\lambda = 0.4$ Å) there are four peaks which probably correspond to the lateral arrangement
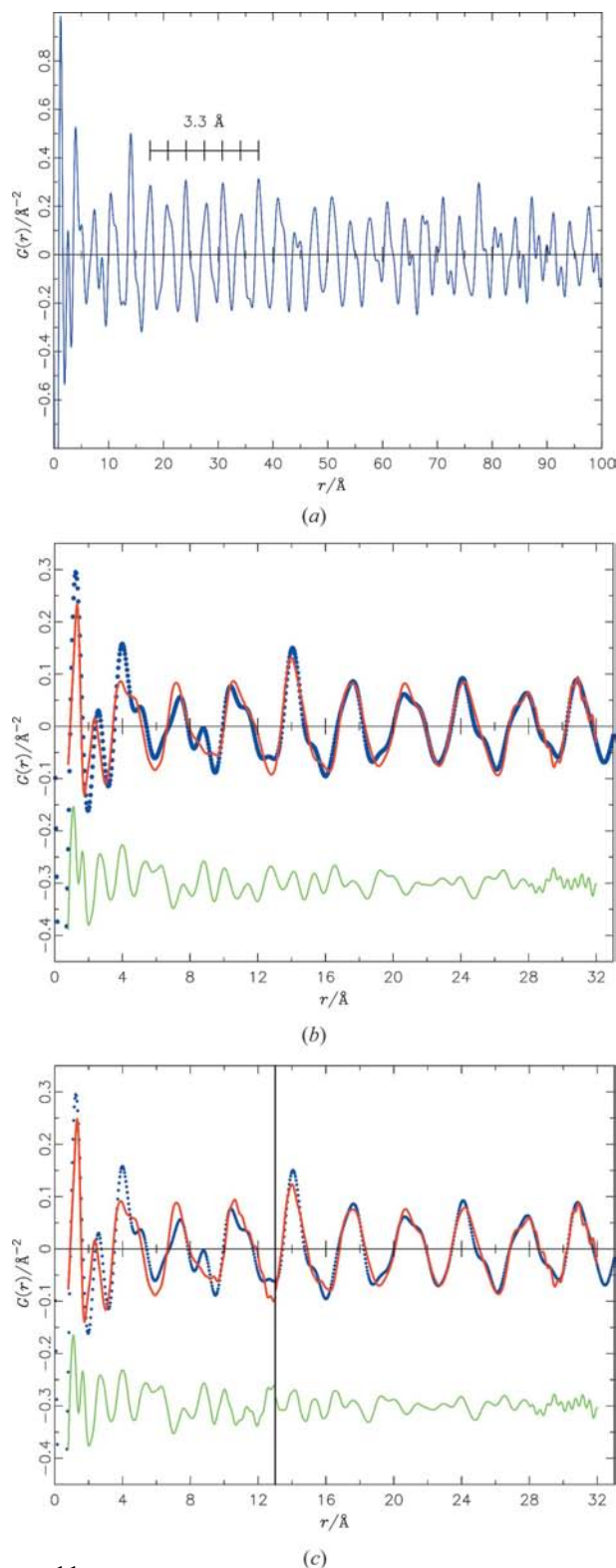

(a)

(b)

(c)

Figure 11
(*a*) PDF or $G(r)$ of α-P.Y. 213; (*b*) PDF fit in the range $0.8 < r < 32$ Å; blue dots: experimental $G(r)$, red solid line: calculated $G(r)$ (only three parameters refined), bottom: difference curve; (*c*) independent PDF fits for the ranges $0.8 < r < 13$ and $13 < r < 32$ Å. This figure is in colour in the electronic version of this paper.

of the columns. From their peak widths the domain size can be estimated to be ~ 200–300 Å. With a column diameter of 10–15 Å this domain size indicates a translational order of ~ 20 columns.

The PDFs of the β and the α phase are virtually identical for $r < 10$ Å, but the similarities cease beyond $r > 13$ Å (Fig. 12*b*). Hence the local structures of the β and the α phases should be similar. This holds for the molecular structure ($r = 0.9$–18 Å) as well as for the arrangement of neighbouring molecules ($r > 3.3$ Å). On the other hand, a change in the molecular conformation (*e.g.* rotation of the COOCH$_3$ group) has only a minor effect on the PDF, thus it remains obscure if the molecules in the α and β phases have the same conformations.

A refinement of the PDF of the β phase would require a structural model. The actual crystal structure of the β-phase is not known; but since the local structures of the phases are similar, we tested to refine the PDF of the β phase using the structural model of the α phase. The character of the PDF of the β phase does not allow for reasonable refinements of the range of $0.8 < r < 32$ Å, nor for $13 < r < 32$ Å. However, the refinement for $0.8 < r < 10$ Å results in $R = 0.485$ (Table 4 and Fig. 12*c*), which compares well to the corresponding region for the α phase ($R = 0.469$). This confirms that the local structures ($r < 10$ Å) are similar. Beyond about $r = 10$ Å, there are major differences in the packings of the α and β phases.

4. Conclusions

The crystallinity of the α phase of P.Y. 213 is at the borderline of being suitable for structure determination from X-ray powder data using the classical approach *via* initial indexing. Electron diffraction turned out to be a quite time-consuming, but very valuable tool for structure solution: we finally obtained the correct indexing from electron-diffraction tilting series (although the lattice was triclinic); on the other hand, the intensity data from electron diffraction were used to test the correctness of structures proposed by lattice-energy minimization. If we had not made a wrong assumption on the molecular conformation, the structure of α-P.Y. 213 would have been solved by the combination of electron diffraction and crystal-structure prediction using lattice-energy minimization. The final successful structure solution from laboratory X-ray powder data proved the power of today's real-space methods. The PDF analysis of the α phase is in agreement with the crystal structure. Although the PDF refinement was carried out with fixed atomic coordinates and lattice parameters, the calculated and experimental PDF curves match well. Software developments have to be carried out to allow a PDF refinement of atomic coordinates for organic compounds including rigid bodies and restraints for bond lengths, bond angles and planar groups, as is available in Rietveld programs nowadays.

The PDF analysis of the nanocrystalline β-phase revealed that this phase adopts a columnar structure with a domain size of below 4 nm in the column direction and a local structure similar to the α phase. These results show that even a poor powder diagram still contains information about the solid-
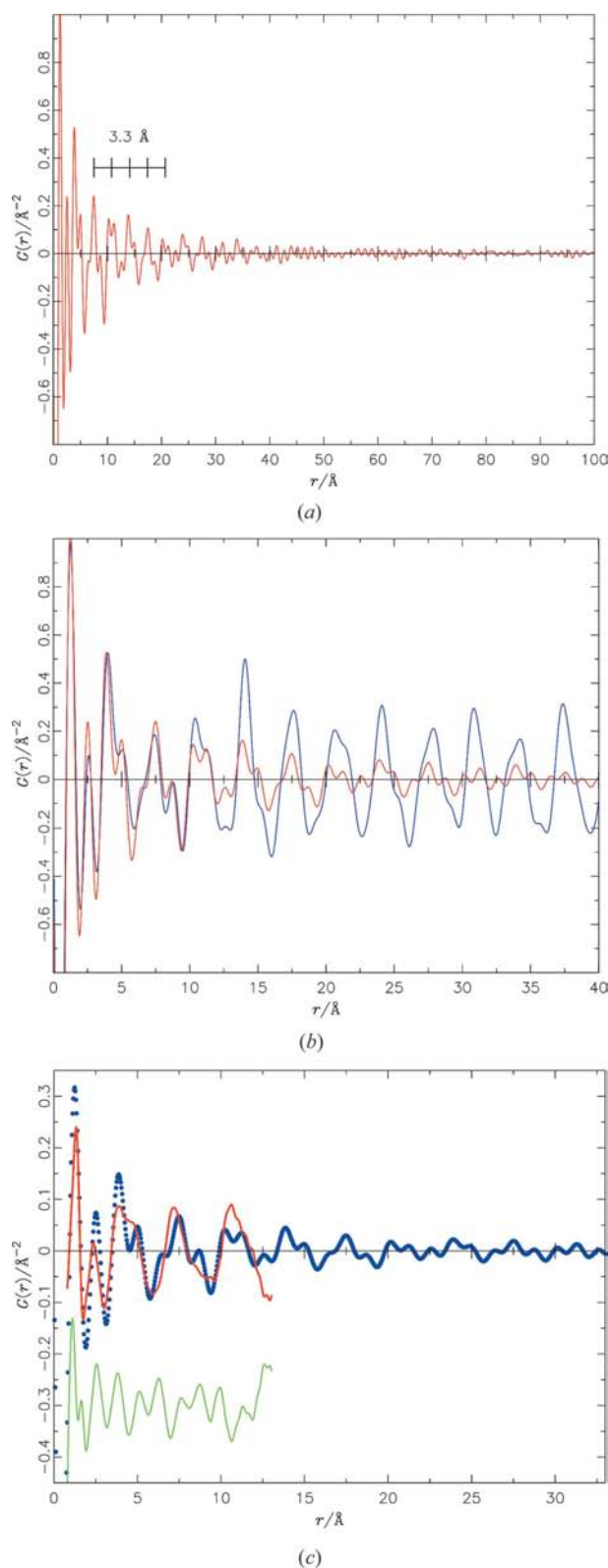
state structure of an organic compound, and this information can be extracted by the PDF method. A PDF analysis for organic crystals is far from being a routine method, but we are convinced that an increasing number of solid-state structures of nanocrystalline organic compounds will be investigated by PDF analysis in the next decade.

Figure 12

(a) PDF or $G(r)$ of β-P.Y. 213. (b) Comparison of PDFs for the α phase (blue) and β phase (red) in the region $r < 40$ Å; note the local resemblance up to $r = 10$ Å. (c) PDF fit of the β phase (thick blue line) using the structural model of the α phase (thin red line) in the range $0.8 < r < 13$ Å. This figure is in colour in the electronic version of this paper.

References

Allen, F. H. (2002). *Acta Cryst.* B**58**, 380–388.
Bates, S. & Ivanisevic, I. (2005). International Patent Application PCT WO 2005082012 A2.
Billinge, S. J. L. & Kanatziolis, M. G. (2004). *Chem. Commun.* pp. 749–760.
Boultif, A. & Louër, D. (1991). *J. Appl. Cryst.* **24**, 987–993.
Brühne, S., Uhrig, E., Kreiner, G. & Assmus, W. (2006). *Philos. Mag.* **86**, 463–468.
Buchsbaum, C. & Schmidt, M. U. (2007). *Acta Cryst.* B**63**, 926–932.
Coelho, A. A. (2006). *TOPAS Academic*, Version 4.0, http://members.optusnet.com.au/~alancoelho/.
David, W. I. F., Shankland, K., van de Streek, J., Pidcock, E., Motherwell, W. D. S. & Cole, J. C. (2006). *J. Appl. Cryst.* **39**, 910–915.
Dollase, W. A. (1986). *J. Appl. Cryst.* **19**, 267–272.
Egami, T. & Billinge, S. J. L. (2003). *Underneath the Bragg Peaks.* Oxford: Pergamon Press.
Gozzo, F., Schmitt, B., Bortolamedi, T., Giannini, C., Guagliardi, C., Lange, M., Meister, D., Maden, D., Willmot, P. & Patterson, B. D. (2004). *J. Alloys Compd.* **362**, 206–217.

Herbst, W. & Hunger, K. (2004). *Industrial Organic Pigments*, 3rd ed. Weinheim: Wiley-VCh.

Hofmann, D. W. M. & Kuleshova, L. (2005). *J. Appl. Cryst.* **38**, 861–866.

Hovmöller, S. (1992). *Ultramicroscopy*, **41**, 121–135.

Jeong, I.-K., Proffen, T., Mohiuddin-Jacobs, F. & Billinge, S. J. L. (1999). *J. Phys. Chem. A*, **103**, 921–924.

Juhas, P., Cherba, D. M., Duxburg, P. M., Punch, W. F. & Billinge, S. J. L. (2006). *Nature*, **440**, 655–658.

Kolb, U. & Gorelik, T. (2005). *Electron Crystallography*, Vol. 211, pp. 421–433. Dordrecht, The Netherlands: Kluwer Academic Publishers.

Kolb, U., Gorelik, T., Kübel, C., Otten, M. T. & Hubert, D. (2007). *Ultramicroscopy*, **107**, 507–513.

Kolb, U., Gorelik, T. & Otten, M. T. (2008). *Ultramicroscopy*, **108**, 763–772.

Kolb, U. & Mateeva, G. N. (2003). *Z. Kristallogr.* **218**, 259–268.

Larson, A. C. & von Dreele, R. B. (1994). *GSAS.* Report LAUR. Los Alamos National Laboratory, New Mexico, USA.

LeBail, A. (2004). *Powder Diffr.* **19**, 249–254.

March, A. (1932). *Z. Kristallogr.* **81**, 285–297.

Mayo, S. L., Olafson, B. D. & Goddard, W. A. III (1990). *J. Phys. Chem.* **94**, 8897–8909.

Nollenberger, K., Gryczke, A., Meier, C., Dressman, J., Schmidt, M. U. & Brühne, S. (2009). *J. Pharm. Sci.* **98**, 1476–1486.

Paulus, E. F., Leusen, F. J. J. & Schmidt, M. U. (2007). *CrystEngComm*, **9**, 131–143.

Proffen, T. & Billinge, S. J. L. (1999). *J. Appl. Cryst.* **32**, 572–575.

Qiu, X., Thompson, J. W. & Billinge, S. J. L. (2004). *J. Appl. Cryst.* **37**, 678.

Schmidt, M. U., Ermrich, M. & Dinnebier, R. E. (2005). *Acta Cryst.* **B61**, 37–45.

Schmidt, M. U., Hofmann, D. W. M., Buchsbaum, C. & Metz, H. J. (2006a). *Angew. Chem.* **118**, 1335–1340.

Schmidt, M. U., Hofmann, D. W. M., Buchsbaum, C. & Metz, H. J. (2006b). *Angew. Chem. Int. Ed.* **45**, 1313–1317.

Schmidt, M. U. & Kalkhof, H. (1997). *CRYSCA.* Frankfurt am Main, Germany.

Schmitt, B., Broennimann, C., Eikenberry, E. F., Huelsen, G., Toyokawa, H., Horisberger, R., Gozzo, F., Patterson, B., Schulze-Briese, C. & Tomikazi, T. (2004). *Nucl. Instrum. Methods Phys. Res. Sect. A*, **518**, 436–439.

Shankland, K., Markvardsen, A. J. & David, W. I. F. (2004). *Z. Kristallogr.* **219**, 857.

Shirley, R. (2006). *CRYSFIRE.* University of Surrey, England.

Stengel-Rutkowski, B. & Metz, H. J. (2001). *Eur. Coat.* **3**, 126–129.

STOE & Cie (2004). *WinXPOW.* STOE and Cie, Darmstadt, Germany.

Streek, J. van de, Brüning, J., Ivashevskaya, S. N., Ermrich, M., Paulus, E. F., Bolte, M. & Schmidt, M. U. (2009). *Acta Cryst.* **B65** 200–211.

Vainstein, B. K. (1964). *Structural Analysis by Electron Diffraction.* Oxford: Pergamon Press.

Visser, J. W. (1969). *J. Appl. Cryst.* **2**, 89–95.

Werner, P.-E., Eriksson, L. & Westdahl, M. (1985). *J. Appl. Cryst.* **18**, 367–370.